Journal of The Electrochemical Society, **152** (9) A1719-A1725 (2005)
0013-4651/2005/152(9)/A1719/7/$7.00 © The Electrochemical Society, Inc.

Electrochemical Characterizations on Si and C-Coated Si Particle Electrodes for Lithium-Ion Batteries

Wei-Ren Liu,[a] Jen-Hao Wang,[a] Hung-Chun Wu,[b] Deng-Tswen Shieh,[b] Mo-Hua Yang,[b,*] and Nae-Lih Wu[a,*,z]

[a]*Department of Chemical Engineering, National Taiwan University, Taipei, Taiwan 106*
[b]*Materials Research Laboratories, ITRI, Chutung, Hsin-Chu, Taiwan 310*

The understanding of cycling and electrochemical characteristics of Si particle anodes for Li-ion batteries has previously been hindered by very fast capacity fading. Optimizing the electrode architecture to significantly improve its stability up to the 1000 mAh/g charge-discharge level has made it possible to investigate these properties to a greater depth than before. The capacity fading and lithiation mechanisms of Si and C-coated Si particles have been studied in this paper by cycling test and electrochemical impedance spectroscopy (EIS) analysis. The capacity vs cycle number plot exhibits two regions of different fading rates, including an initial region of slow fading followed by accelerated decay. The latter may be associated with large-scale failure of the electrode structure. EIS revealed a core-shell lithiation mechanism of Si. C-coating not only exerts remarkable favorable effects against capacity fading, but also serves as a conduit for Li ions to the reaction with Si particles.
 [DOI: 10.1149/1.1954967]

Manuscript submitted January 22, 2005; revised manuscript received March 22, 2005. Available electronically July 21, 2005.

As one approach to increase the electrical storage capacity for the Li-ion secondary battery, a vast amount of work has been devoted to replace the graphite anode with new materials that form alloys with Li. Among them, silicon is an attractive candidate due to its potentially very large capacity, over 3000 mAh/g.[1,2] The application of Si anode, nevertheless, has been hindered by rapid capacity fading upon charge-discharge (C-D) cycling. Although the fading is apparently associated with the dramatic volumetric variation upon the alloying/dealloying reactions with Li, the current understanding of the mechanistic mechanism to such failure in fact remains vague, and the interplay between the architecture of a Si particle electrode and its cycle life has yet to be systematically explored. In addition, although there has been an increasing amount of literature on basic electrochemical properties of thin-film electrodes of Si and its alloys[3-6] in recent years, information for the Si particle electrode is scarce. This is partly because it has indeed been difficult to achieve long enough cycle life for detailed characterization.

It has been demonstrated in our previous studies[7,8] that the amount of conductive graphitic/carbonaceous additives and the type of binder material have significant effects on the stability of the Si particle anode. By optimizing these electrode architecture factors, significant enhancement in the cycling stability of Si particle anodes has been made. This has made it possible for us to carry out electrochemical characterizations on this type of Si electrode to a greater extent than before.

In addition, great enthusiasm has also been shown to coat the Si particles with secondary materials, which may serve either to increase the conductivity of the electrode or to be a buffer that can partially accommodate the volumetric variation.[9-13] Among these secondary materials, including C, oxides, and nitrides, only coating with graphite/C has so far shown a promising effect,[9-11] but the role of C has not been elucidated.

In this work, the electrochemical properties of Si and carbon-coated Si (which is hereafter abbreviated as C-Si) particle electrodes have been studied mainly by C-D cycling test and electrochemical impedance spectroscopy (EIS) analyses. In brief, two fading modes for Si anode have been identified, including a local one due to loss of electronic contact between individual particles and a global mode due to failure of the entire electrode structure. Coating of Si particles with conductive C was found to effectively suppress the local fading and improve structural stability. C-D potential data along with impedance analysis indicate that lithiation of Si proceeds via the formation of Li_xSi layers with different x values within Si particles, and the C coating can serve as an intermediate conduit of Li ions before reacting with Si particles.

* Electrochemical Society Active Member.
z E-mail: n1w001@ntu.edu.tw

Experimental

Sample preparation.— The Si powder employed has an average size of ~3 μm with 85% of the particles being smaller than 5 μm.[7] It was obtained by ballmilling a 20-μm starting powder purchased from Aldrich (99%). Wet ballmilling was carried out in a polyethylene jar containing an ethanol-water (95:5) solution and two different Al_2O_3 balls that are of 5 and 2 mm diam, respectively, and at a rotation speed of 300 rpm for 24 h. C-Si powder was prepared by a fluidized-bed type of chemical vapor deposition (CVD). In a typical run, carrier gas, N_2, was bubbled through a benzene reservoir and then directed to a vertical reactor, where the Si powder was loaded. To enable fluidization of the powder, an electromagnetic valve was used to produce pulsed flow. The deposition process was carried out at 900°C. The C-Si particles were gently ground and sieved before electrode preparation.

Electrode and coin-cell preparation.— The Si electrodes were constituted of, on the dry basis, 62 wt % active material (i.e., Si or C-Si), 30 wt % conductive additives, and 8 wt % binder. The binder was a mixture of styrene-butadiene-rubber (SBR; L1571, Asahi Chemicals) and sodium-carboxyl-methyl-cellulose (SCMC; WS-C, Cellogen, DKS International, Inc.) with 1:1 weight ratio. The conductive additives included graphitic flakes (KS6, 3 μm, Timcal) and nanosized carbon black (Super P, 40 nm, Timcal) with a weight ratio of 5:1. The mixed slurry was coated on Cu foil with a final film thickness of ~50 μm. CR2032 coin cells were fabricated from the Si and C-Si electrodes. The counter electrode was lithium foil. The electrolyte was 1 M $LiPF_6$ in ethylene carbonate (EC): ethyl methyl carbonate (EMC) (1:2). All the potentials reported herein are referenced to Li/Li^+.

Electrochemical and material characterizations.— A C-D cycle consisted of the steps of (*i*) discharging (lithiating) at a constant current (CC) of 0.3 mA/mg until either the selected specific capacity (mAh/g) or the zero-potential bound was reached, and (*ii*) charging (delithiating) at 0.3 mA/mg until the cutoff voltage (1.2 V) was reached. An equilibrating period of 5 h was adopted at the end of the first discharging.

For EIS analysis, each coin cell was consecutively charged or discharged to different levels at which impedance spectra were taken. The cell was allowed to equilibrate for 30 min before each spectrum was taken. An Autolab frequency response analyzer (Autolab, Eco Chenie PGSTAT30) was employed for obtaining the spectra within the frequency range from 5 mHz to 60 kHz. The

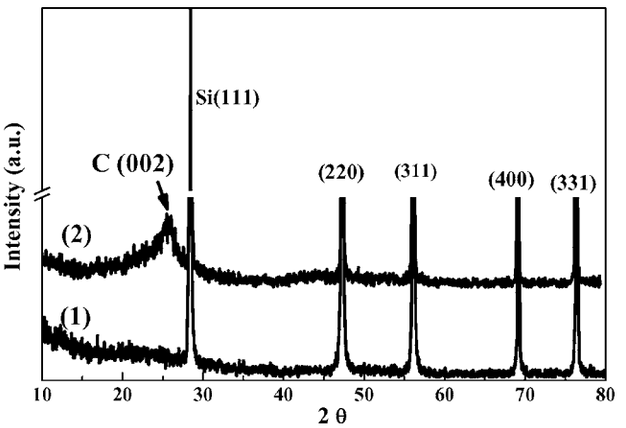

Figure 1. XRD patterns of (1) Si and (2) C-coated Si particles.

resistance across the electrode (overlay + Cu) was also measured by using the four-point method. It is clear that the resistance is contributed mainly by the overlay.

Thermal gravimetrical analysis (TGA) was performed by using an Ulvac TGD-7000 at a scanning rate of 5°C/min to determine the amount of C coating. Particle morphologies were examined by scanning electron microscopy (SEM; LEO1530). Cross-sectional microstructures of the C-coating layer were examined by transmission electron microscopy (TEM; JEM-2010). X-ray diffraction (XRD) was carried out on a Mac-Science/MXP diffractometer with Cu Kα radiation. Raman scattering (Olympus BH2-UMA) was measured at room temperature on a Renishaw 2000 micro-Raman Fourier transform spectrometer using an Ar^+ laser at 514 nm as the excitation source.

Results and Discussion

XRD patterns of pure silicon and carbon-coated silicon were presented in Fig. 1. The presence of the C coating was evidenced by the presence of a broad (002) peak at $2\theta \sim 25°$, which is close to the (002) reflection of graphite. However, the d-spacing of this peak is 0.350 nm, in contrast to 0.335 nm for graphite, suggesting defected crystalline structure. Raman spectroscopy analysis indicated only ~50% graphene bonding coordination (Fig. 2).

TGA analysis indicated that the C-Si particles contain 27 wt % C. SEM micrographs show that while the surface of the Si particle is smooth (Fig. 3a), the C coating exhibits a granular surface morphology (Fig. 3b and c). More importantly, the coating shows excellent conformity and uniformity in thickness. Cross-sectional TEM

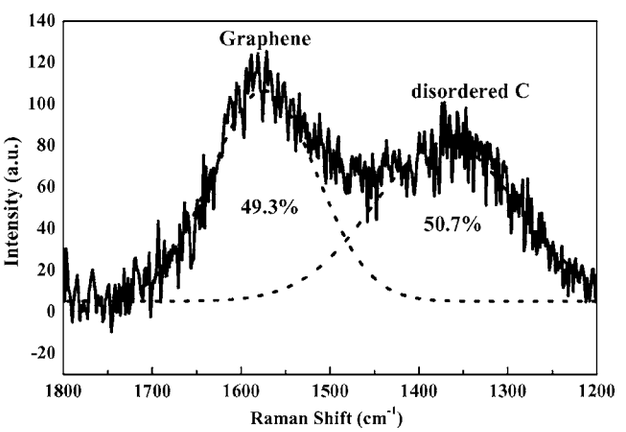

Figure 2. Raman spectrum showing the bonding structure of the C-coating.

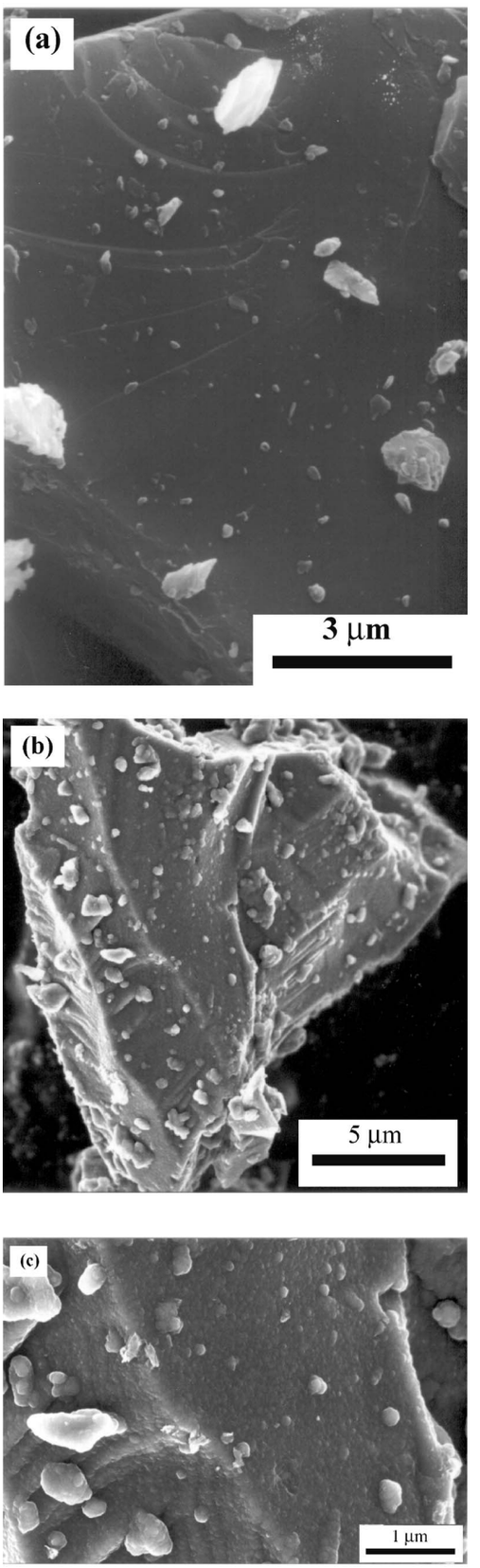

Figure 3. SEM micrographs of (a) Si and (b, c) C-Si particles, showing conformal deposition of granular C-coating on Si.

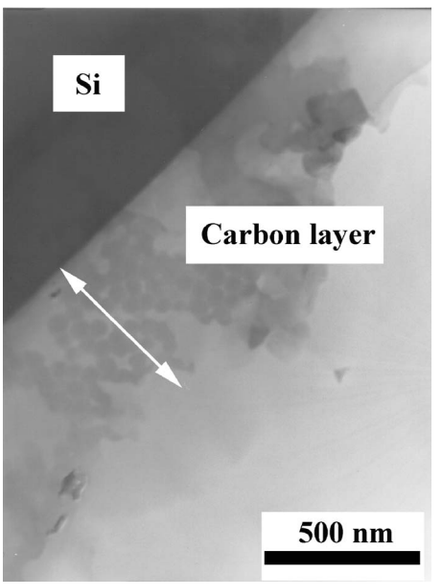

Figure 4. Cross-sectional TEM image of the C-coating on Si particle.

(Fig. 4) identified that the C coating has a thickness of ~500 nm and contains granules of ~50 nm diam. These microstructural data basically showed that uniform coating of disordered C has been achieved by the CVD process utilizing the pulsed-flow, fluidized-bed technique.

Figures 5 and 6 summarize the discharge (lithiation) and charge (delithiation) capacity data for the Si and C-Si electrodes, respectively, while Fig. 7 showed the potential curves of selected cycles. Two designated discharge levels, 800 and 1000 mAh/g, have been tested for either electrode. The designated discharge capacities were calculated by taking into account solely the active material, either Si or the C-Si particles, in the electrode. The graphitic component of the conductive additives, KS6, was checked to have a capacity of ~170 mAh/g. [This value is lower than that (340 mAh/g) previously reported by Winter et al.[14] The difference may be caused by different C-D current densities employed. Current densities of 0.01 mA/mg during the first circle followed by 0.1 mA/mg in the rest cycles was employed in the previous study, while 0.3 mAh/mg was used here.] Furthermore, as shown later, the C coating was

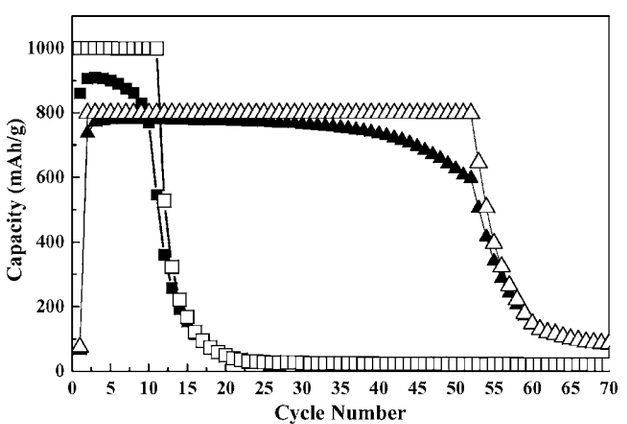

Figure 5. Capacity vs cycle number plots for Si electrode at designated discharge capacities of 800 and 1000 mAh/g. The open symbols are for discharge (lithiation) capacities, and the solid symbols for charge (delithiation) capacities.

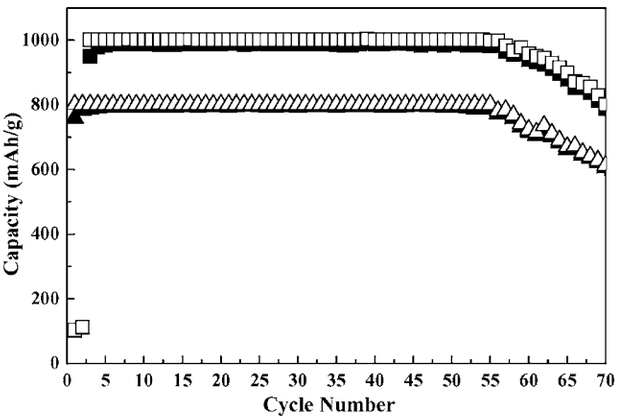

Figure 6. Capacity vs cycle number plots for C-Si electrode at designated discharge capacities of 800 and 1000 mAh/g. The open symbols are for discharge (lithiation) capacies, and the solid symbols for charge (delithiation) capacities.

estimated to contribute a capacity of ~30 mAh/g C-Si. By taking these contributions into account, Table I lists the estimated discharge capacities of the Si phase in either electrode under the designated discharge capacities. For the Si electrode, the true discharge capacity of the Si particle is smaller than the designated value due to the contribution of the conductive additives. For the C-Si electrode, it is reversed because the C-coating never contributes as much capacity as the Si phase. As an example, in the case of designated discharge capacity of 800 mAh/g (C-Si), subtracting the contribution (~69 mAh/g) due to the K26 graphitic additive gives the true discharge capacity of 731 mAh/g for the C-Si particles. The discharge capacity of the Si component, Y (mAh/g Si), of the composite particles can then be calculated by the following equation

$$Y \times (1\text{-}27 \text{ wt } \%) = (731 - 30) \text{ mAh/g}$$

which gives Y of 960 mAh/g Si, as shown in Table I.

At the designated discharge capacity of 800 mAh/g for Si (Fig. 5), fading in charge (dealloying) capacity commenced at the 25th cycle. Before that, the electrode showed coulombic efficiencies better than 95%. Beyond the 25th cycle, two fading regimes can be identified. The first regime occurred between the 25th and 52nd cycles, where the designated discharge capacity level can be reached but the coulombic efficiency starts to fall. That is, although Li ions are allowed to react with sufficient Si to reach the designated depth (800 mAh/g), not all of them are released during charge. The results

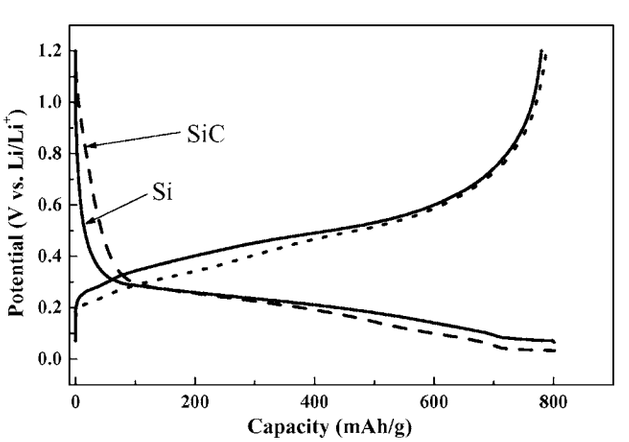

Figure 7. Potential vs capacity plots for (solid line) Si electrode and (dashed) C-Si electrode.

Table I. Estimated discharge capacities of the Si phase in the Si and C-Si electrodes.

Electrode	Designated discharge capacity (mAh/g)	Discharge capacity of Si (mAh/g)[a]
Si	800	731
Si	1000	931
C-Si	800	960
C-Si	1000	1275

[a] The capacities are calculated based on a capacity of 170 mAh/g for the KS6 graphitic additive and a capacity of 30 mAh/g C-Si contributed by the C coating.

indicate that the Si particles are always in good contact with the conductive additives during discharge, but some individual particles begin to lose contact with the conductive additives upon charge. This is mainly because the volumes of the particles are expanding during lithiation, while they start to shrink upon delithiation. This fading mode can be considered as a local mode which is associated with individual particles.

The second regime occurs beyond the 52nd cycle, where the designated discharge capacity can no longer be reached (Fig. 5). That is, there are not sufficient Si particles in good contact with the conductive additives even during discharge, and it suggests that the entire structure of the electrode became severely loosened and crumbled. This may be referred to as a global mode and is associated with the failure of the entire electrode architecture. It can be seen that, once getting into this mode, the electrode completely failed within a few cycles (Fig. 5). In essence, the local fading mode is characterized by the attainment of the designated discharge capac-

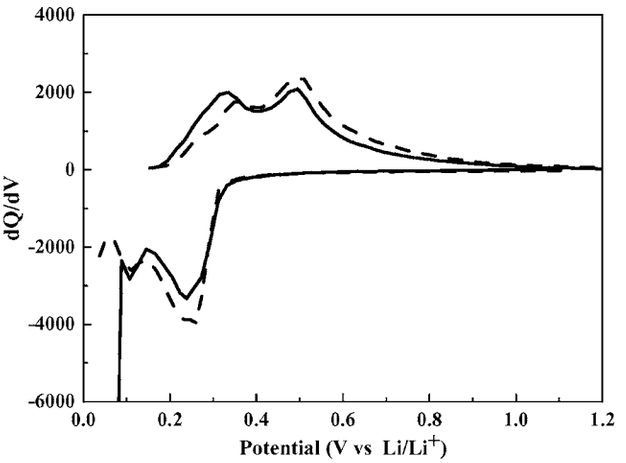

Figure 8. Differential capacity plots for (solid line) Si electrode and (dashed) C-Si electrode.

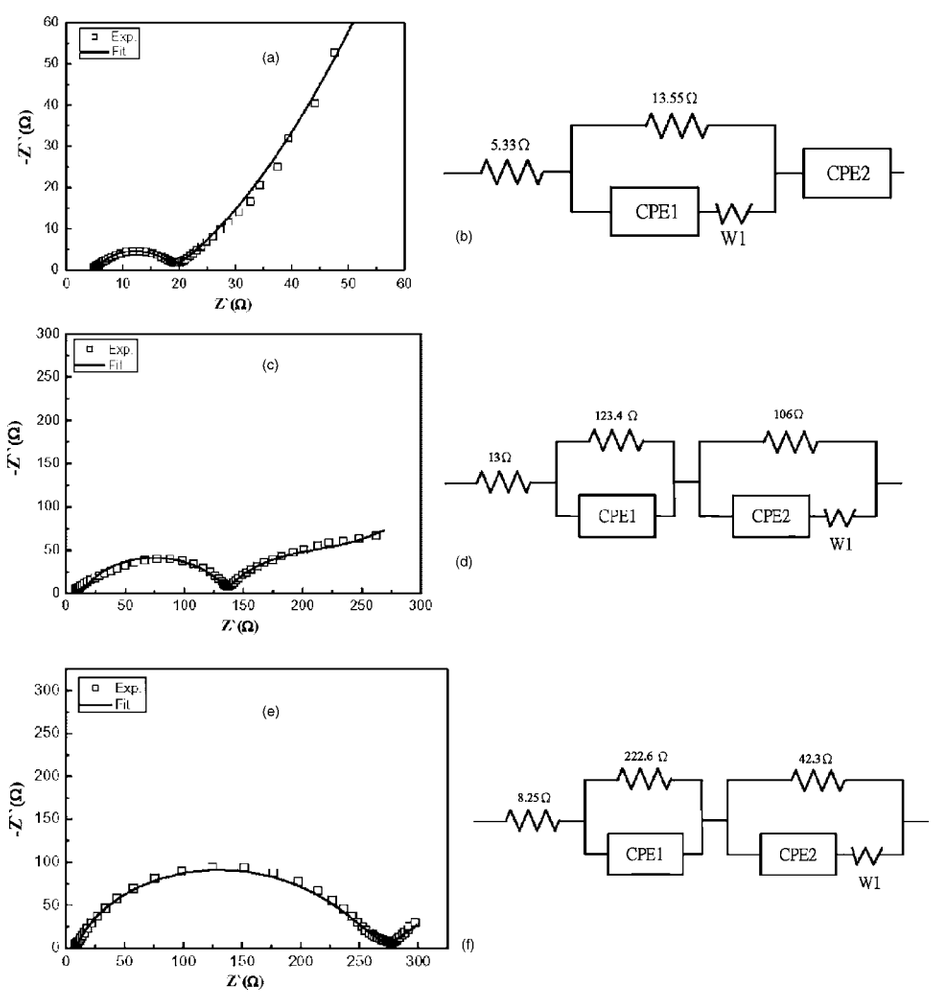

Figure 9. EIS spectra and equivalent circuits for Si electrode: (a, b) 100 mAh/g; (c, d) 400 mAh/g; (e, f) 600 mAh/g.

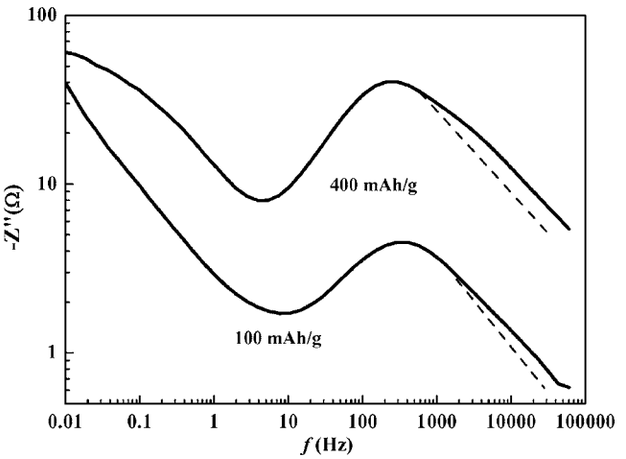

Figure 10. Impedance imaginary component ($-Z''$) vs frequency (f) plots for the Si electrode at discharge depths of 100 and 400 mAh/g, respectively. The dashed lines are drawn in order to elucidate the presence of a shoulder in the curve within the high-f region.

ity in combination with a coulombic efficiency being significantly less than unity. The global fading mode is by accelerated declination in attainable discharge capacity.

Using the features shown in the capacity vs cycle number plot that are associated with fading mechanism, we can now see how different factors influence the cycling stability of the Si electrode. For example, as shown in Fig. 5, the discharged depth has a significant effect on the occurrence of both local and global fading modes. For the designated discharge capacity of 1000 mAh/g, the local mode commences at the very beginning of the cycling test, while the global mode set in at the 10th cycle. Both occurred much earlier than for 800 mAh/g. As shown in Fig. 6, the C-Si showed only the global fading mode but not the local one. It means that the Si particles, either fresh or fractured by reactions, are mostly in good contact with conductive materials within the electrode until the entire structure of the electrode started to fail. In addition, the global fading mode proceeds at slower rate (vs cycle number) for the C-coated Si. That is, the entire electrode structure of the C-Si electrode is mechanically more stable and "tolerating" toward volume variations during cycling. The C-Si electrode shows overall remarkably improved cycling stability than the Si electrode, particularly for the high discharge depth. At 1000 mAh/g, the C-Si electrode did not exhibit fading until the 57th cycle, in contrast to complete fading at the 8th cycle for the Si electrode.

Accordingly, the C-D data have suggested two effects due to the C-coating. First, the skip of the local fading mode suggests that the coating serves to form an exquisite conductive network to allow the fractured Si particles to remain in good electronic connection with one another. Such a network cannot be achieved by mechanical mixing of Si particles and conductive additives. The resistance measured across the electrode (overlay + Cu) was found to be reduced by more than 50%, from 55 $\mu\Omega$ for Si to 26 $\mu\Omega$ for C-Si, by the presence of the surface carbon coating. Second, the C coating could serve as a buffer to partially accommodate the volume variation during the C-D cycling so that the stability of the entire electrode structure can be improved.

It is also interesting to notice that, for either Si or the C-Si electrode, it in some cases took a couple of "induction" cycles to reach the full designated discharge capacity (e.g., for Si at 800 mAh/g in Fig. 5 or C-Si at 1000 mAh/g in Fig. 6). This induction phenomenon, which has not been observed when polyvinylidene fluoride is used as the binder, is believed to arise from incomplete wetting of the electrolyte solution within the electrode. This is a particular problem needing extra precaution when a water-based binder, such as SBR, is employed. Nevertheless, even during these induction cycles, the irreversible capacity is less than 10 mAh/g.

The Si electrode typically showed an inclined plateau for either the discharge or charge branch of the potential vs capacity curves (Fig. 7). The differential capacity plot (dQ/dV vs capacity) identifies one major broad peak between 0.35 and 0.15 V followed by a small peak at $\sim$0.1 V during discharge (Fig. 8). The 0.1 V peak can be attributed to lithiation of the KS6 component of the conductive additive mixture, as confirmed by control study using the KS6 electrode. The broad peak is associated with lithiation of the Si phase and is believed to result from overlapping of at least two reaction events, in view of the two delithaition peaks appearing in the charge branch. The line profiles of the differential capacity plots are consistent with those reported for amorphous Si thin-film electrodes in the literature.[4,6]

For the C-Si electrode, there was observed additional insertion of Li ions between 0.3 and 1.1 V (Fig. 7) as compared with the Si. Cyclic voltammetry analysis confirmed the reversibility of the reaction(s) within this potential range. It has also been previously observed by Yoshio et al.[10,11] and can be attributed to lithiation/delithiation of disordered C, i.e., of the C coating.[15] By shifting the potential curve of the C-Si electrode horizontally toward the lower capacity direction, the curve was found to coincide perfectly with the curve of the Si electrode within the potential range between 0.5 and 0.25 V, i.e., the onset of the reaction plateau of the Si electrode. The differential capacity curves of the C-Si electrode exhibited essentially the same peak features as the Si electrode below 0.5 V (Fig. 8). It is thus concluded that contribution of the C coating in coulombic capacity is negligible below 0.5 V. Accordingly, the capacity contributed by the C coating is estimated to be the capacity difference between these two curves at 0.5 V, and it is $\sim$30 mAh/g (C-Si). At lower potential range (ca. $<$0.3 V), both the discharge and charge branches of the C-Si potential curve lie below those of the Si curve. This is not related to polarization but simply because the true capacity of the Si phase in the C-Si electrode is in fact always higher than that in the Si electrode under the same calculated discharge/charge depth.

The impedance spectra were acquired along the course of a C-D cycle with the designated discharge capacity of 600 mAh/g. Upon being charged or discharged to a selected state, a spectrum was acquired after the cell was allowed to equilibrate for 0.5 h. It was found that for both the Si and C-Si cells, reproducible trend was not established until the second cycle. The data described below were taken during the second cycle for each electrode.

For the Si electrode at 1.2 V, there is detected only an inclined line which corresponds to an equivalent circuit consisting of a constant phase element (CPE). The spectrum indicates that there is essentially no lithiation reaction taking place at this potential. Upon discharge to 100 mAh/g (0.29 V) (Fig. 9a), the spectrum shows a depressed semicircle followed by an inclined line. Figure 10 shows the $-Z''$ (imaginary component of the impedance) vs f (frequency) plot of the spectrum in logarithm scale, showing a peak within the f-range associated with the semicircle. Theoretically, if the semicircle is associated with only one process, each of the two branches of the peak should have an asymptote of straight line. However, there is noted the presence of a shoulder along the high-f branch of the peak, indicating the presence of an additional process. This shoulder, in fact, becomes increasingly clear with increasing discharge depth (e.g., 400 mAh/g in Fig. 10). The data indicate that there are at least two, but not one, events involved with the semicircle. Analogous to lithiation of graphite, the impedance toward the high-f end may be attributed to the solid/electrolyte interface thin-film on the Si surface, while the impedance within the intermediate-f region, which constitutes major part of the semicircle, is due to charge-transfer. As the high-f event is always small, it is therefore neglected in the subsequent simulation study for simplicity. By doing so, the Nyquist plot for the discharge depth of 100 mAh/g can be satisfactorily simulated by a circuit consisting of an electrolyte

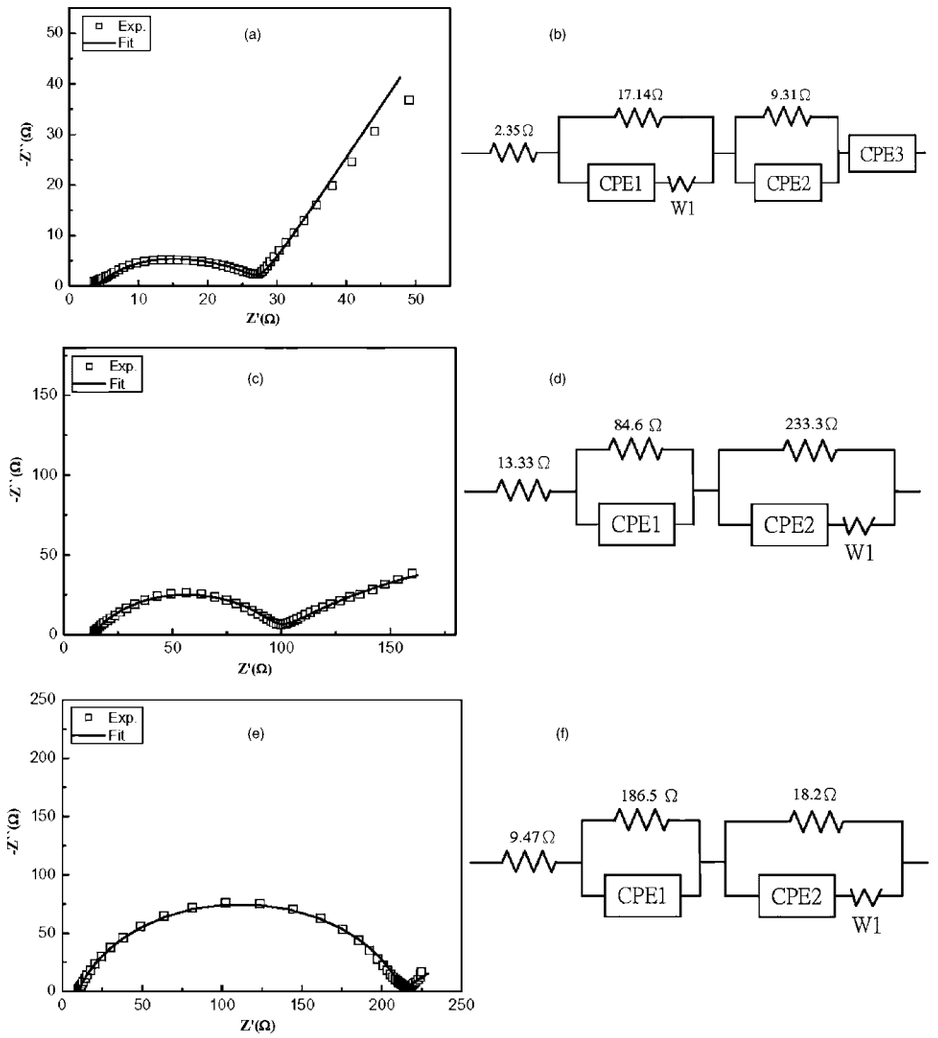

Figure 11. EIS spectra and equivalent circuits for C-Si electrode: (a, b) 100 mAh/g; (c, d) 400 mAh/g; (e, f) 600 mAh/g.

resistance in series with a Randles-type impedance element and a blocking CPE (Fig. 9b). CPE, rather than ideal capacitor, has been introduced in order to simulate the depressed nature of the intermediate-f semicircle and the nonideality of the blocking capacitance at the low-f end. One possible origin for the CPE characteristics might arise from the porous nature of the electrode.[16]

At the discharge of 400 mAh/g (Fig. 9c), the spectrum shows the following distinct differences from the 100 mAh/g spectrum. First, the resistance of the intermediate-f semicircle increases significantly, by nearly eightfold. Second, the low-f line becomes much more curved. The spectrum can no longer be fitted with the 100 mAh/g circuit. Rather, the spectrum can be well fitted by the circuit including an R//C element in series with a Randles-type impedance element (Fig. 9d). The spectrum at 600 mAh/g (Fig. 9e) is qualitatively similar to the 400 mAh/g one in line profile, showing mainly a depressed semicircuit followed by a curved line toward the low-f end. Accordingly, it can be fitted by using the same equivalent circuit as the 400 mAh/g spectrum, which consists of two impedance elements in series, in combination with a significant increase adjustment in resistance of the first impedance element (Fig. 9f).

The 100 mAh/g equivalent circuit (Fig. 9b) can be interpreted as the formation of a lithiated layer extending from the surface into the interior of the Si particle. The Randles impedance element of the circuit represents the charge-transfer impedance for the Li ion getting into the Si particle, while the CPE element arises from the presence of the unlithiated Si core. For the equivalent circuit of 400 mAh/g (Fig. 9d), the presence of two impedance elements may be interpreted as the charge-transfer impedances of two lithiated Si regions, including an inner Li-lean core (the Randles element) with a lower Li solubility and an outer Li-rich shell (the R//C element) with a higher Li solubility range. That is, a core-shell layer structure consisting of Li_xSi of different x values is established. The 600 mAh/g circuit (Fig. 9f) suggests that the core-shell structure remains except that there is perhaps an increase in layer thickness of the outer Li_xSi shell and that the charge-transfer resistance associated with this outer layer increases rapidly with increasing Li-ion content.

In their microstructural study on lithiated Si particles by high-resolution TEM, Limthongkul et al.[17] reported the observations of amorphization of Si by the electrochemically driven lithiation and the coexistence of an amorphous surface layer with a central core of crystalline Si within individual Si particles. The latter gives support to the proposed equivalent circuit for the discharge depth of 100 mAh/g as described above (Fig. 9b). From the kinetic point of view, the core-shell structure in fact suggests that the lithiation process is limited by diffusion of Li ions, in contrast to being limited by interfacial reaction, and the apparent reaction rate can be described by an unreacted-core shrinking model.[18] Free Gibbs energy calculation[17] has also indicated that amorphization upon lithiation, rather than formation of crystalline Li-Si alloys, is not due to thermodynamic consideration but to slow crystallization kinetics. In this case, one would expect the amorphized region to have a Si-Li sto-

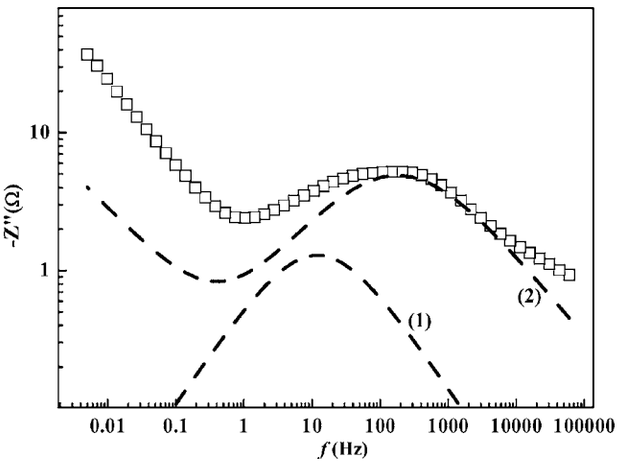

Figure 12. Impedance imaginary component ($-Z''$) vs frequency plots for the C-Si electrode at the discharge depth of 100 mAh/g. The dashed lines are the simulated results from, respectively, the R//C and Randles impedance elements shown in the equivalent circuit in Fig. 11b.

ichiometry close to any of the known Li-Si alloys (but fails to crystallize). As there are more than one crystalline Li-Si alloys known to exist,[1] more than one amorphous layer having different Li contents could hence coexist during the course of lithiation. The proposed core-shell structure may also explain the occurrence of more than one delithation peak appearing in the differential capacity plots (Fig. 8).

For the C-Si electrode at the discharge depth of 100 mAh/g, the Nyquist plot (Fig. 11a) showed a depressed circle followed by a straight line, similar to that of the Si electrode at the same designated discharge depth. However, the plot of ($-Z''$) vs f indicated a distinct difference between the electrodes, namely, an additional event within the range between 1 and 100 Hz for the C-Si electrode (Fig. 12), and this event must have to do with the C coating. Previous reports[19,20] have indicated that the charge-transfer impedance for Li intercalation into either graphitic or disordered C has the characteristic frequency in the range of 1–50 Hz, and thus this additional event may be attributed to the charge-transfer impedance associated with the C coating. These results indicate that at higher potentials, Li ions preferentially first intercalate into the C coating and then move into Si. Accordingly, the spectrum can be well simulated by a circuit consisting of an R//C impedance element additional to the circuit of the 100 mAh/g circuit of Si (Fig. 11b and Fig. 12). This additional R//C element reflects the charge-transfer impedance associated with Li ion getting into the C-coating.

At the designated discharge depths of 400 and 600 mAh/g, the impedance plots of the C-Si electrode (Fig. 11c and e) show qualitatively the same line profiles as those of Si electrode, i.e., no additional reaction event as described above was detected, and therefore they can be simulated by the same type of equivalent circuits (Fig. 11d and f). That is, the same lithiation mechanism takes places in both electrodes at higher discharge depths. Physically it means that lithiation by direct reaction of Li ions at the Si/electrolyte interface without routing through the C coating becomes predominant below a certain potential threshold. The same core-shell structure described above for the uncoated Si particles is also expected to exist within the C-coated Si particles.

Conclusions

The capacity vs cycle number plot of the Si particle electrode was found to provide features serving as a useful guide to elucidating two fading modes, including a local mode arising from loss of electronic contact of individual particles with the conductive network of the electrode and a global mode that arises from failure of the entire electrode structure. Surface coating of the Si particles with conductive C material was found not only to effectively suppress the local fading mode but also improve the stability against the global fading mode. The C-D potential vs capacity data and EIS analysis indicate that lithiation of Si proceeds via a series of reactions that result in core-shell structure of Li_xSi with different x values within Si particles. The C coating can serve as an intermediate conduit of Li ions before their reacting with Si particles.

Acknowledgment

This work is supported by the National Science Council of Taiwan, Republic of China, under contract no. NSC93-ET-7-002-001-ET.

The National Taiwan University assisted in meeting the publication costs of this article.

References

1. C. J. Wen and R. A. Huggins, *Solid State Chem.* **37**, 271 (1981).
2. M. N. Obrovac and L. Christensen, *Electrochem. Solid-State Lett.*, **7**, A93 (2004).
3. H. Yagi and H. Tarui, U.S. Pat. 6,649,033 B2 (2003).
4. L. Y. Beaulieu, T. D. Hatchard, A. Bonakdarpour, M. D. Fleischauer, and J. R. Dahn, *J. Electrochem. Soc.*, **150**, A1457 (2003).
5. J. Graetz, C. C. Ahn, R. Yazami, and B. Fultz, *Electrochem. Solid-State Lett.*, **6**, A194 (2003).
6. T. D. Hatchard and J. R. Dahn, *J. Electrochem. Soc.*, **151**, A838 (2004).
7. W.-R. Liu, Z.-Z. Guo, D.-T. Shieh, H.-C. Wu, M.-H. Yang, and N.-L. Wu, *J. Power Sources*, **140**, 139 (2005).
8. W.-R. Liu, Z.-Z. Guo, D.-T. Shieh, H.-C. Wu, M.-H. Yang, and N.-L. Wu, *Electrochem. Solid-State Lett.*, **8**, A100 (2005).
9. T. Umeno and K. Fukuda, EP Pat. 1024544 A2 (2000).
10. M. Yoshio, H. Wang, K. Fukuda, T. Umeno, N. Dimov, and Z. Ogumi, *J. Electrochem. Soc.*, **149**, A1598 (2002).
11. N. Dimov, K. Fukuda, T. Umeno, S. Kugino, and M. Yoshio, *J. Power Sources*, **114**, 88 (2003).
12. II-seok Kim, G. E. Blomgren, and P. N. Kumta, *Electrochem. Solid-State Lett.*, **6**, A157 (2003).
13. G. A. Robert, E. J. Cairns, and J. A. Reimer, *J. Power Sources*, **110**, 424 (2002).
14. M. Winter, P. Novak, and A. Monnier, *J. Electrochem. Soc.*, **145**, 428 (1998).
15. J. R. Dahn, T. Zheng, Y. Liu, and J. S. Xue, *Science*, **270**, 590 (1995).
16. R. de Levie, *Electrochim. Acta*, **9**, 1231 (1964).
17. P. Limthongkul, Y.-I. Jang, N. J. Dudney, and Y. M. Chiang, *J. Power Sources*, **119**, 604 (2003).
18. M. Ishida and C. Y. Wen, *AIChE J.*, **14**, 311 (1968).
19. Z. Ogumi, T. Abe, T. Fukutsuka, S. Yamate, and Y. Iriyama, *J. Power Sources*, **127**, 72 (2004).
20. A. Funabiki, M. Inaba, and Z. Ogumi, *J. Power Sources*, **68**, 227 (1997).